DOI: 10.13009/EUCASS2023-042
Aerospace Europe Conference 2023 – 10TH EUCASS – 9TH CEAS

Steady 1D Viscous Non-Adiabatic Flow Model for the Determination of Inner Geometry and Power Density Profile of Nuclear Fuel Element

*Elia Puccinelli**† and Angelo Pasini**
* Department of Civil and Industrial Engineering, University of Pisa
elia.puccinelli@phd.unipi.it – angelo.pasini@unipi.it
† Corresponding Author

Abstract
The present work represents the first step toward a new layout for the nuclear propulsion systems. The regenerative cooled nozzle present in the historic configuration is eliminated from the system and replaced with several smaller nozzles shaped inside each core's coolant channels. The focus of this study is the determination of the channel's optimum geometry for a general fuel element and the corresponding power density distribution. These outputs are achieved by implementing a new methodology for solving the 1D steady viscous and non-adiabatic duct flow equations by imposing the Mach number and the wall outer temperature profiles as boundary conditions.

Nomenclature

A= Duct Cross Section
A_e= Nozzle Exit Area
C_f= Friction Coefficient
C_h= Stanton Number
C_p= Specific Heat
D= Duct Diameter
F= Friction Force
F_{thrust}= Thrust Force
g_o= Gravitational Acceleration
I_{sp}= Specific Impulse
k= Flow Thermal Conductivity
k_{fuel}= Fuel Thermal Conductivity
L_{cc}= Fuel Element Length
$\dot{m}$= Mass Flow Rate
M= Mach Number
M_e= Flow Exiting Mach Number
NTP= Nuclear Thermal propulsion
NTR= Nuclear Thermal Rocket
Nu= Nusselt Number
ODE= Ordinary Differential Equation
P= Duct Perimeter
p= Static Pressure
$P(z)$= Nuclear Reactor Power Density
p_a= Ambient Pressure
p_e= Nozzle Exit Pressure
p_{in}= Flow Initial Pressure
p_t= Stagnation Pressure
Pr= Prandtl Number
$\dot{Q}$= Heat Exchanged
R=Gas Constant
r= Channel Radius
Re= Reynolds Number
r_i= Channel Inner Radius
r_o= Channel Outer Radius
T_{bulk}= Flow Bulk Temperature
T_e= Nozzle Exit Temperature
T_{in}= Flow Initial Temperature
T_{max}= Fuel Maximum Limiting Temperature
T_r= Wall Radial Temperature Distribution
TRL= Technology Readiness Level
T_t= Stagnation Temperature
T_w= Duct Wall Temperature
u= Flow Velocity
u_e= Flow Exiting Velocity
x= Coolant Channel Axis Abscissa
γ= Specific Heat Ratio
μ= Bulk Flow Viscosity
μ_w= Wall Flow Viscosity
ρ= Density

DOI: 10.13009/EUCASS2023-042

1. Introduction

The nuclear thermal rocket's historic configuration foresees the use of prismatic nuclear fuel elements displaced in several rings composing the reactor's core. A turbopump assembly pumps the propellant through the coolant channels craved inside each fuel element absorbing the heat generated by the nuclear core. Then the hot propellant from each fuel element collects inside a thrust chamber and expands through a regenerative cooled bell-shaped nozzle. This configuration was the one that reached the highest TRL from the 1960s until today, but several different solutions have been proposed through the years [1–5]. One of the main purposes of the various proposed configurations was the reduction of the propulsion system mass and envelope respect to the one first developed in the frame of the Rover/NERVA program in the U.S. One possible approach to reduce the propulsion system axial envelope and complexity is the substitution of the single cooled nozzle with several small nozzles. In particular, the idea behind this work is the replacement of the single nozzle with multiple nozzles integrated inside each of the coolant channels inserted in the fission reactor core, as illustrated in Figure 1. Some authors proposed in the literature a similar configuration [5,6], however, no one focuses on the determination of the craved nozzle geometry inside the coolant channels crossed by a viscous non-adiabatic flow; the friction is not negligible in a duct with a radius in the order of millimeters, and the determination of the heat entering inside the propellant flow is a key factor in the design of these propulsion systems. These two source factors make the flow through the channel not isentropic, causing more difficulties in generating the nozzle geometry inside each channel for maximizing the thrust. In the case of isentropic flow, the Rao Method [7] allows to obtain the bell-shaped nozzle contour maximizing the propulsion system thrust through the Method of the Characteristics after imposing the nozzle length, inlet conditions, and ambient pressure. The proposed approach utilizes the Rao method only as a starting point for determining a first-tentative Mach number profile along the channel axis. Then the methodology moves to the solution of a system of two ordinary differential equations for determining the properties of a non-isentropic flow and the coolant channel and nozzle contour.

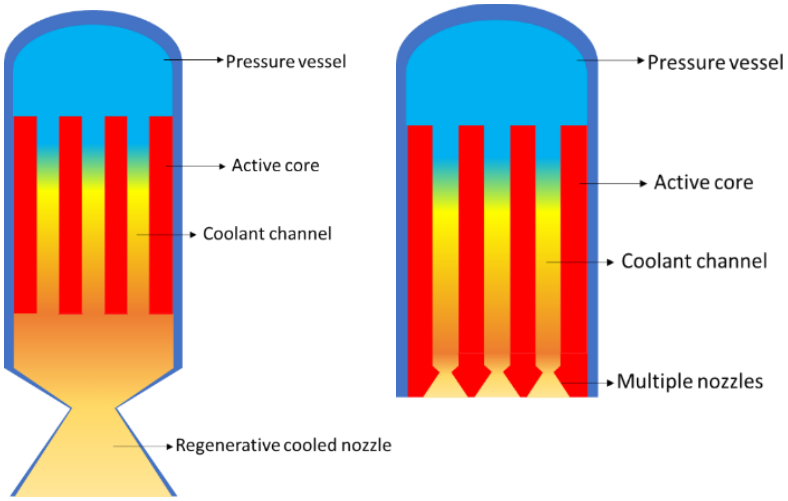

Figure 1: Single (left) and Multiple (right) Nozzle Nuclear Thermal Rocket Configurations

.

2. Methodology

The multiphysical analysis for characterizing the performance of a nuclear thermal rocket uses the results of the neutronics analysis of the fission reactor configuration to determine the power density profile along the core radius and axis; the obtained profile serves as a boundary condition for the thermal-hydraulics analysis, which gives as an output the temperature distribution of the core and the flowing through propellant. These two steps are repeated iteratively until convergence. This work treats only the thermal-hydraulic part of the analysis focusing only on the section related to the propulsive performance of the problem. Following this strategy, no assumption constrains the type of nuclear fission reactor and fuel elements. Whichever the fuel element configuration, the coolant channel element can be approximated as a cylindrical duct with heat generated inside the walls due to the fission reaction of the fuel material; this is true also in the case of a prismatic fuel element, as the one used in the Rover/NERVA program, through the approximation process depicted in Figure 2. Therefore, a general cylindrical duct with an unknown inner radius profile along the channel axis represents the analyzed case. Figure 3 illustrates the channel element subject of the study; the channel terminates with a nozzle craved directly inside the propellant duct, and the contour of this nozzle constitutes another unknown of the problem to be determined while solving the flow equations. The ordinary differential equations

DOI: 10.13009/EUCASS2023-042

characterizing the steady 1D non-adiabatic viscous duct flow represent the analyzed problem; Eq.(1) reports this system of equations.

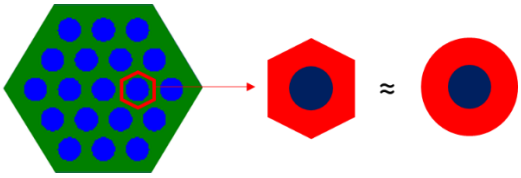

Figure 2: Coolant Channel Element Cylindrical Duct Approximation

$$\begin{cases} \dfrac{dT_t}{T_t} = \dfrac{d\dot{Q}}{\rho u A c_p T_t} \\ \dfrac{dp_t}{p_t} = -\dfrac{dF}{pA} - \dfrac{\gamma}{2} M^2 \dfrac{d\dot{Q}}{\rho u A c_p T_t} \\ \dfrac{dM}{M} = -\dfrac{1+\frac{\gamma-1}{2}M^2}{1-M^2}\dfrac{dA}{A} + \dfrac{1+\frac{\gamma-1}{2}M^2}{1-M^2}\dfrac{dF}{pA} \\ \quad + \dfrac{\frac{1}{2}(\gamma M^2+1)\left(1+\frac{\gamma-1}{2}M^2\right)}{1-M^2}\dfrac{d\dot{Q}}{\rho u A c_p T_t} \end{cases} \tag{1}$$

Figure 3 also reports the main parameters, the boundary conditions, and the known quantities assumed for the solution of this system of equations. The temperature and pressure at the inlet of the duct (p_{in}, T_{in}) and the required mass flow rate ($\dot{m}$) are assumed as known inlet properties of the flow and determined starting from values generally accepted in the literature for this class of propulsion systems [1,8]. The mass flow rate remains constant and equal to the inlet value along the overall channel length due to the absence of suction and injection of fluid at the duct's walls. The literature indicates a suitable first tentative value for the outer radius (r_o), the length of the fuel element, and, consequently, the coolant channel element (L_{cc}). The vacuum conditions on which the engine will operate impose the value for the ambient pressure (p_a); Table 1 reports the value associated with these known quantities.

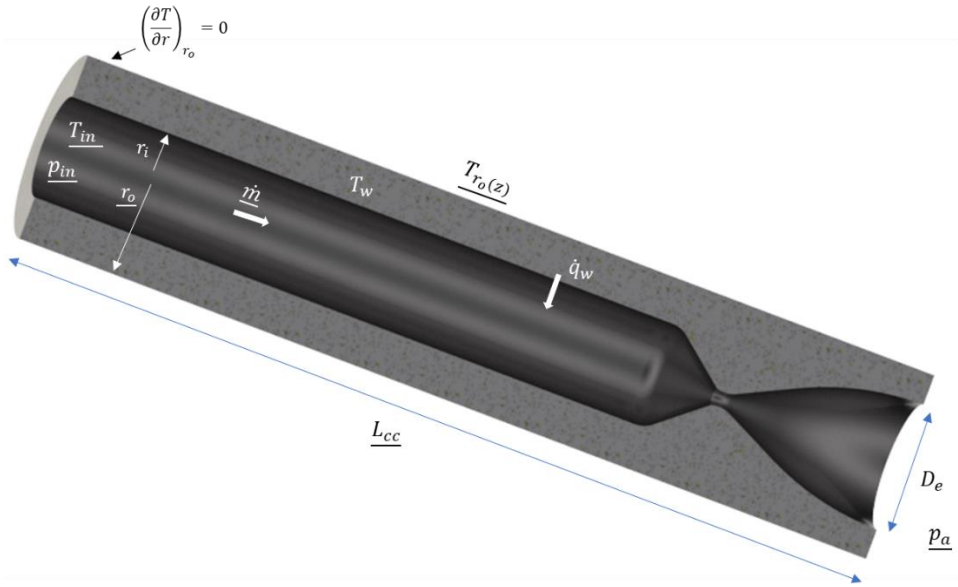

Figure 3: NTR Coolant Channel Element with Integrated Nozzle

The ε_{conv} parameter in the table represents the ratio between the inlet radius of the channel and the nozzle throat radius (the minimum radius achieved along the duct). The choice of the value of this quantity is arbitrary and can be adjusted to obtain different performance values. The other two main assumptions shown in the table for the solution of the system of the equations are related to the propellant and fuel selection. Ammonia represents the selected propellant for this study based on the results of a previous review [9]. This choice goes somewhat against what is recommended in the literature since, although ammonia is among the propellants proposed for NTP, most studies consider hydrogen as

DOI: 10.13009/EUCASS2023-042

the propellant due to the low molecular weight of this substance, which guarantees extraordinary performance to the propulsion system. However, hydrogen has many problems, represented by its fugacity, material compatibility, and storage. For this reason, the choice fell on ammonia, which, while providing a specific impulse equal to about half that of hydrogen with the same design and engine outlet temperature, requires much less complex systems for its storage and guarantees a smaller footprint than systems using hydrogen. The ammonia properties as a function of the fluid temperature come from the NIST Database [10]. These functions allow us to simulate the fluid as a thermally perfect gas. As for the nuclear fuel, the principle of not selecting a specific core configuration induces not specifying the material used in this analysis. However, the two most promising types of fuel materials present in the literature are the CerCer and the CerMet, and even if the properties of these materials vary a lot depending on the specific composition, the choice of limit temperature (T_{max}) and thermal conductivity (k_{fuel}) values fell on average values that are found in the literature on NTP for these materials. Finally, the introduced hypothesis of adiabaticity along the channel axis direction and at the outer radius of the element forces the power generated by each infinitesimal fuel volume composing the duct walls to go only in the inner radial direction towards the propellant flow ($\dot{q}_w \neq 0$).

Table 1: Known and Boundary Quantities of the Analysis

Parameter	**Value**
T_{in}	500 K
p_{in}	60 bar
$\dot{m}$	1.43 g/s
ε_{conv}	10
p_a	20 mbar
L_{CC}	1 m
r_o	5 mm
Propellant	Ammonia
γ	1.32
R	488.21 J/kgK
Fuel	CerCer / CerMet
T_{max}	3100 K
k_{fuel}	30 W/mK

Eq.(2) allows to rewrite the source terms governing the total pressure and temperature in Eq.(1) in terms of the friction coefficient (C_f) and Stanton number (C_h), and the diameter of the duct, which represent the four unknowns of the problem (the other three are the flow total pressure (p_t) and temperature (T_t) and the Mach number (M)).

$$\frac{dF}{pA} = \frac{\gamma M^2 C_f P dx}{2A} \qquad \frac{d\dot{Q}}{\rho u A c_p T_t} = \frac{C_h (T_w - T_t) P dx}{A T_t} \tag{2}$$

Eq.(3) lets to write the diameter of the duct's inner wall as a function of the other three unknowns of the problem and the fixed parameters of propellant properties and mass flow rate. In this way, the system of ordinary differential equations becomes a square solvable system.

$$D = \sqrt{\frac{4\dot{m}}{\pi p_t M}\sqrt{\frac{RT_t}{\gamma}}\left(1 + \frac{\gamma - 1}{2}M^2\right)^{\frac{\gamma+1}{2(\gamma-1)}}} \tag{3}$$

The last challenge to face in solving the system of three ODEs is the treatment of the singularity point in the Mach equation (Eq.(4)) when approaching the sonic section of the duct (x_{sp}).

DOI: 10.13009/EUCASS2023-042

$$\frac{dM}{M} = -\frac{1+\frac{\gamma-1}{2}M^2}{1-M^2}2\frac{D'}{D}dx + \frac{1+\frac{\gamma-1}{2}M^2}{1-M^2}\left(\frac{\gamma M^2}{2}C_f\frac{4}{D}dx\right) + \frac{\frac{1}{2}(\gamma M^2+1)\left(1+\frac{\gamma-1}{2}M^2\right)}{1-M^2}\left(C_h\left(\frac{T_w}{T_t}-1\right)\frac{4}{D}dx\right) \quad \textbf{(4)}$$

The approach proposed in this work to deal with this complication differs from what is generally proposed in the literature [11], as the equation is not solved using approximations close to the sonic point but is eliminated from the problem. Introducing a given Mach number profile along the channel axis adds a further constraint to the problem, allowing the corresponding differential equation (Eq.(4)) to be eliminated. The Mach number profile selection is arbitrary and depends on the desired performance at the nozzle outlet. The technique chosen in this study for determining the profile catches on Rao Method [7]. The Rao's method uses the Method of the Characteristics for determining the supersonic nozzle contour that generates the optimum thrust for the given inlet conditions. This approach uses the isentropic flow assumptions through the nozzle. For this reason, it can not be applied directly to the analyzed problem to determine the geometry of the channel and the nozzle. Nevertheless, this new strategy applies the Rao method to the idealized problem considering the flow as isentropic. In this way, the ideal nozzle geometry optimizing the thrust is obtained, and the correspondent ideal Mach number profile along the channel axis is extrapolated. The ideal-case Mach number profile constitutes input information into the viscous non-adiabatic system of equations. It is worth stressing that this distribution is only a first tentative profile; the developed model allows for inserting any Mach number profile as a driver of the problem.

$$\begin{aligned}
\frac{dT_t}{dx} &= +C_h\left(\frac{T_w(x)}{T_t}-1\right)\frac{4T_t}{\sqrt{\frac{4\dot{m}}{\pi p_t M(x)}\sqrt{\frac{RT_t}{\gamma}}\left(1+\frac{\gamma-1}{2}M(x)^2\right)^{\frac{\gamma+1}{2(\gamma-1)}}}} \\
\frac{dp_t}{dx} &= -\frac{\gamma[M(x)]^2}{2}\left[C_f + C_h\left(\frac{T_w(x)}{T_t}-1\right)\right]\frac{4p_t}{\sqrt{\frac{4\dot{m}}{\pi p_t M(x)}\sqrt{\frac{RT_t}{\gamma}}\left(1+\frac{\gamma-1}{2}[M(x)]^2\right)^{\frac{\gamma+1}{2(\gamma-1)}}}}
\end{aligned} \quad \textbf{(5)}$$

Eq.(5) is a system of the ordinary differential equations in the two unknowns of the problem (p_t, T_t) obtained after implementing the aforementioned strategy for the Mach number profile determination. The literature [12] suggests the formulas (Eq.(6)) for the Stanton number and friction factor definition inside the channels of a nuclear reactor.

$$C_h = \frac{Nu}{PrRe}$$

$$\begin{cases}
Nu = 0.023(Re^{0.8})(Pr^{0.4}) & (T_w - T_{bulk}) < 100\ K \\
Nu = 0.023(Re^{0.8})\left(Pr^{\frac{1}{3}}\right) & 100\ \text{K} \leq\ (T_w - T_{bulk}) \leq 1000\ K \\
Nu = 0.023(Re^{0.8})(Pr^{0.4})\left(\frac{\mu_w(T_w)}{\mu(T)}\right)^{0.14} & (T_w - T_{bulk}) > 1000\ K
\end{cases} \quad \textbf{(6)}$$

Where the Reynolds and Prandtl number are defined as:

$$Re = \frac{4\dot{m}}{\pi D\mu(T)}$$

$$Pr = \frac{\mu(T)c_p(T)}{k(T)}$$

And the friction factor:

$$C_f \rightarrow \begin{cases}
C_f = \dfrac{16}{Re_D} & Re_D \leq 2100 \\
\dfrac{1}{\sqrt{4C_f}} = 1.14 + 2\log_{10}\left(Re_D\sqrt{4C_f}\right) & Re_D > 2100
\end{cases}$$

The only information missing for the closure of the problem is the channel wall temperature profile ($T_w(x)$). In the classical approach followed by most of the coupled neutronic-thermal-hydraulics analyses, this temperature is written

DOI: 10.13009/EUCASS2023-042

as a function of the fluid stagnation temperature and the power density profile ($P(z)$) of the fission reactor obtained from the neutronics of the system, as highlighted in Eq.(7).

$$T_w = T_t + \frac{DP(z)A_{duct}}{4\dot{m}c_p C_h} \tag{1}$$

The typical power density profile generated by a NERVA-like fission reactor presents a Bessel function-like distribution in the radial direction and a sine-shaped distribution in the axial direction, as shown in Figure *4*. Looking at the axial power density profile, this generates a temperature distribution along each fuel element such that only a restricted portion of the nuclear fuel reaches the material-limiting temperature. In this way, the fuel presents regions with very different temperatures along its axis, and most of these regions work at a limited temperature to not pose any fuel vaporization risk in the maximum temperature region. Figure *4* shows the typical temperature profiles inside the fuel element. In the present study, the thermal-hydraulics aspects of the analysis are decoupled from the neutronics ones, and the fission reactor does not present a fixed configuration. Therefore, the reactor power density does not constitute a boundary condition of the problem but an unknown.

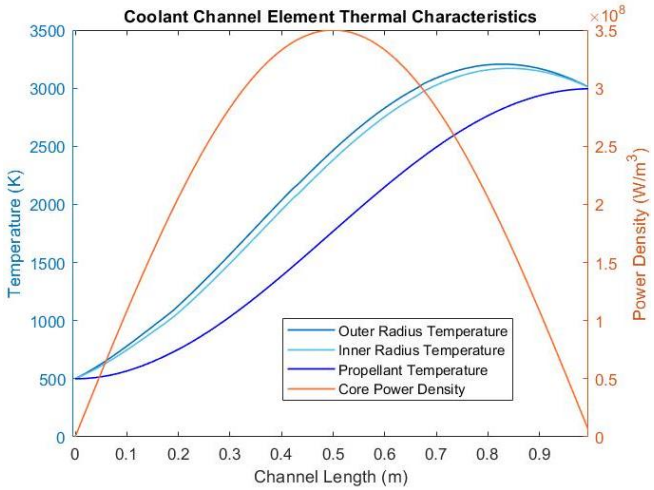

Figure 4: Power Density Profile and Temperature Distribution along Fuel Element Axis

Treating the power density profile along the fuel element axis as an unknown of the problem forces the introduction of a new boundary condition for closing the ODE's system. The strategy of obtaining better performance from the propulsive system chose this new condition to go to the edge of the temperature profile along the outer wall of the coolant channel element. Different temperature profiles can be applied in this region; however, the temperature should be as uniform as possible to make the best use of nuclear fuel.

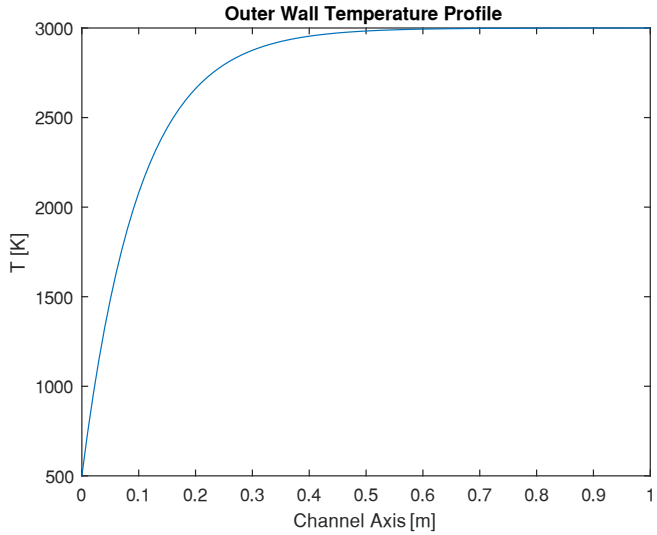

Figure 5: Fixed Outer Radius Temperature Profile

DOI: 10.13009/EUCASS2023-042

A constant temperature along the axis of the channel and equal to the temperature limit of the material might seem the best choice. However, in the inlet area of the flow into the channel, where the propellant has the minimum temperature (T_{in}), the fuel does not need to have these high-temperature values since the heat transferred to the fluid is high even with lower temperatures. For this reason, a temperature trend at the outer radius of the coolant channel wall, like the one shown in Figure 5, constitutes the most effective for having most of the fuel element operating at the maximum possible temperature; Eq.(8) represents the formula implemented for that profile.

$$T_{ro} = T_{max} - (T_{max} - T_{in}) \exp\left(-\frac{x}{h}\right) \tag{2}$$

Where *h* represents a characteristic length fixed arbitrarily to 0.1 m ($= 0.1L_{cc}$).
The outer wall temperature profile enables the writing of the wall's inner radius temperature (T_w) and the core's power density profile ($P(z)$) as a function of the problem's unknowns. Considering an infinitesimal fuel element inside the coolant channel wall, the steady conduction equation for this element can be written as reported in Eq.(9). The integration of this differential equation gives the duct's wall temperature as a function of the radius of the channel up to two constants of integration (*a* and *b*).

$$\begin{gathered} k\left(\frac{1}{r}\frac{\partial}{\partial r}\left(r\frac{\partial T}{\partial r}\right)\right) = -P(z) \\ T = -\frac{P(z)}{k}\frac{r^2}{4} + a\ln(r) + b \end{gathered} \tag{9}$$

The computation of $P(z), a,$ and b is necessary for the determination of the formula of the temperature at the wall's inner radius (r_i). The insertion of the boundary conditions generates a system of three algebraic equations in the three unknowns (Eq.(10)), which can be put in matrix form and solved obtaining the inner wall temperature and the power density profile as a function of the other two unknowns of the original ODE's system (T_t, p_t).

$$\begin{cases} -\dfrac{P(z)}{4k_{fuel}}r_o^2 + aln(r_o) + b = T_{ro} \\ -\dfrac{P(z)}{2k_{fuel}}r_o + \dfrac{a}{r_o} = 0 \\ -\dfrac{P(z)}{4k_{fuel}}r_i^2 + aln(r_i) + b - T_t = -\dfrac{P(z)A_{duct}}{2C_h\dot{m}c_p}r_i + \dfrac{ak_{fuel}A_{duct}}{r_iC_h\dot{m}c_p} \end{cases} \tag{3}$$

$$\begin{Bmatrix} P(z) \\ a(z) \\ b(z) \end{Bmatrix} = \begin{bmatrix} \dfrac{-1}{4k_{fuel}}r_o^2 & ln(r_o) & 1 \\ \dfrac{-1}{2k_{fuel}}r_o & \dfrac{1}{r_o} & 0 \\ \dfrac{r_iA_{duct}}{2C_h\dot{m}c_p} - \dfrac{1}{4k_{fuel}}r_i^2 & ln(r_i) - \dfrac{k_{fuel}A_{duct}}{r_iC_h\dot{m}c_p} & 1 \end{bmatrix}^{-1} \begin{Bmatrix} T_{ro}(z) \\ 0 \\ T_t(z) \end{Bmatrix} \tag{4}$$

After this last step, every term in Eq.(5) is a function of the two unknowns (or a known value) of the problem, and the two ordinary differential equations can be numerically integrated to obtain the flow properties along the coolant channel element from which Eq.(12) estimates the propulsive performance, and Eq.(13) determines the radial temperature distribution inside the coolant channel element which represents a boundary condition for the subsequent neutronic analysis. The other two main outputs of the problem are the channel geometry ($r_i(z)\ or\ D(z)$) and the core's power density profile ($P(z)$).

$$T_e = T_{te}\left(1 + \frac{\gamma - 1}{2}M_e^2\right)^{-1} \tag{12}$$

DOI: 10.13009/EUCASS2023-042

$$u_e = M_e\sqrt{\gamma R T_e}$$

$$F_{thrust} = \dot{m}u_e + (p_e - p_a)A_e$$

$$I_{sp} = \frac{F_{thrust}}{\dot{m}g_o}$$

$$T_r(r,z) = \frac{P(z)}{4k_{fuel}}(r_i^2 - r^2) + r^2 \ln\left(\frac{r}{r_i}\right) + T_{ri}(z) \quad \textbf{(5)}$$

The first one gives the bell-shaped nozzle geometry to be machined inside each of the core's fuel elements, while the second one represents a constraint for the fission reactor configuration; obtaining the reactor's power density profile as an output of the thermal-hydraulic analysis instead of the neutronics analysis pushes to design the fission reactor following precise fuel temperature requirements, which are connected to the propulsive performance. The next steps of this procedure will be the determination of the reactor's configuration and the correspondent neutronic analysis to assess its criticality.

3. Results and discussion

Figure *6* shows the Mach number profile along the channel axis obtained after imposing the isentropic conditions on the problem and obtaining the channel Rao geometry maximizing the thrust of the system for the imposed conditions at the inlet section.

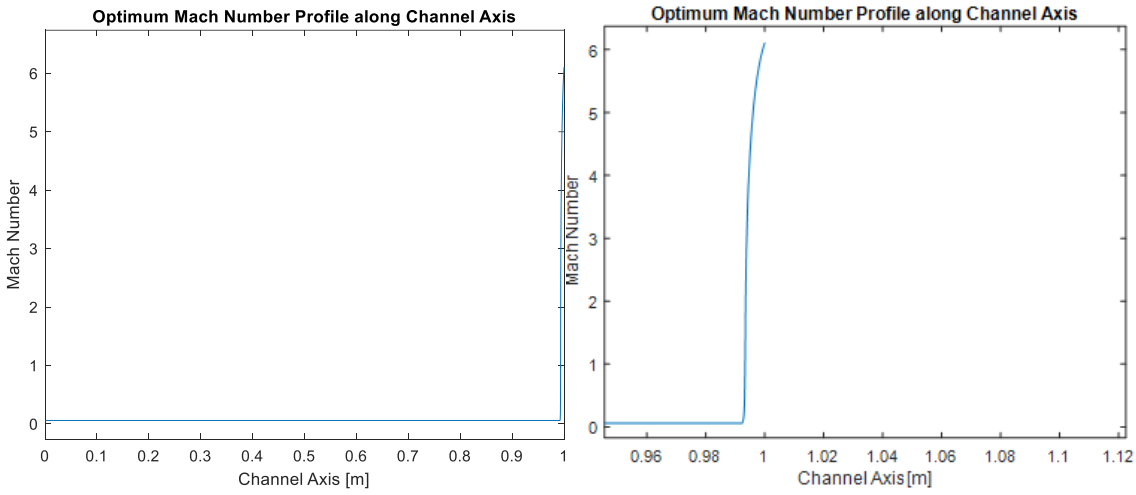

Figure 6: Imposed Mach Number along the Channel Axis

Figure *7* shows the channel geometry obtained by numerically solving the system of ordinary differential equations after imposing as a boundary condition the Mach number profile shown in the figure above. The inner radius of the channel slowly increases while proceeding from the channel inlet to the outlet, and when it approaches the end of the channel (after 0.99 m), it assumes the shape of a bell nozzle. This profile is in accordance with the imposed Mach number profile along the channel axis; as the Mach shall remain constant, the duct radius must increase to counteract the accelerating effect of the heat introduced in a subsonic flow, and the duct assumes a convergent-divergent nozzle shape as the Mach number suddenly increases and surpasses the sonic value close to the channel outlet section. Looking at the right-hand side of the figure, the exit diameter and the aperture angle of the obtained nozzle geometry are larger than the ones derived in the isentropic case applying the Rao method due to the higher internal energy of the exiting gas. Figure *8* illustrates the static and stagnation pressure profiles along the duct. As expected, the pressure slowly decreases before the divergent part of the nozzle due to the effect of heat addition inside the flow, while the contribution of the friction is almost negligible due to the very low Mach numbers characterizing this trait of the duct; in the convergent-divergent nozzle, the pressure suddenly decreases due to the enhanced friction effect accompanying the increase of the Mach number. The extremely low dimensions of the nozzle's diameters contribute to magnifying these

DOI: 10.13009/EUCASS2023-042

pressure losses beyond the 15 bar. The supersonic portion of the nozzle is considered adiabatic to partially counteract the pressure losses by eliminating the negative contribution of the heat addition. This hypothesis is also in line with the layout generally proposed for most the fission reactor: as shown in Figure *9* for the case of a prismatic fuel element, the final segment of the fuel elements composing the fission reactor is made of non-nuclear material for structure supporting reasons. In this way, considering the ending portion of the fuel element, the one corresponding to the sections occupied by the divergent part of the nozzle, is a reasonable assumption.

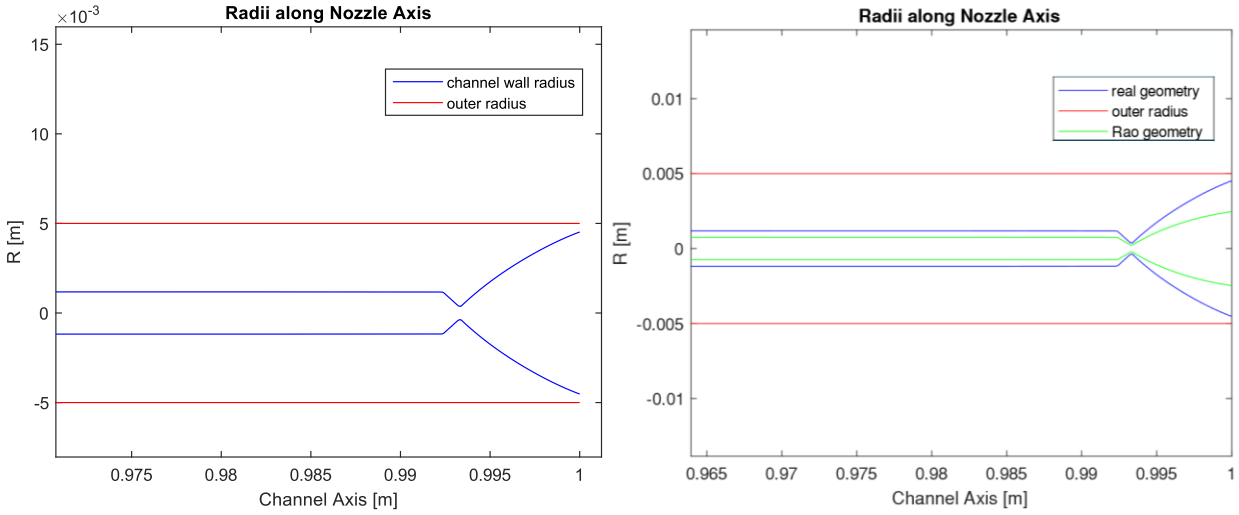

Figure 7: Coolant Channel Geometry with Integrated Nozzle (left) and Comparison with Rao Geometry (right)

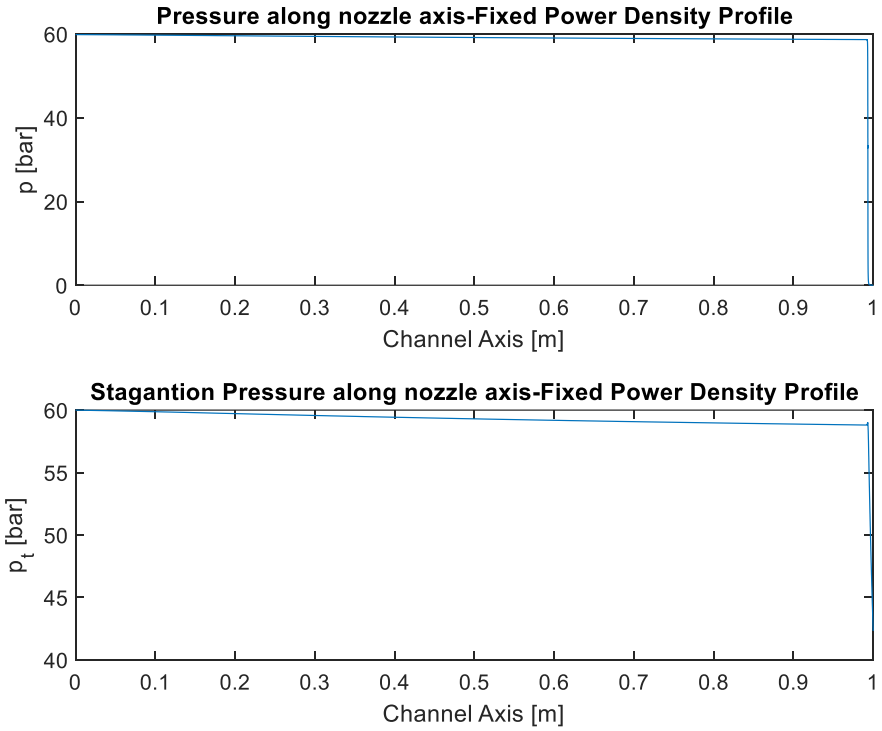

Figure 8: Static (upper) and Stagnation (lower) Pressure Profiles along Channel Axis

DOI: 10.13009/EUCASS2023-042

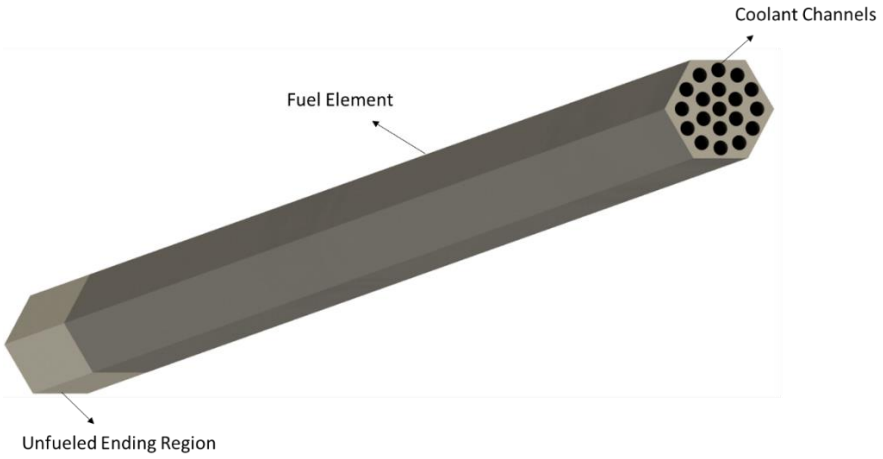

Figure 9: Prismatic Fuel Element Fueled and Unfueled Regions

Figure 10 depicts the static and stagnation temperature profile along the coolant channel axis. The stagnation temperature increases from the duct inlet to the duct outlet thanks to the heating from the channel walls, while the static temperature profile resembles the stagnation temperatures one up to the section where the converging part of the nozzle begins due to the negligible dynamic contribution. The flow's static temperature suddenly decreases in the divergent part of the nozzle since the internal energy of the flow is converted into kinetic energy for the exiting gas acceleration. The stagnation temperature remains constant in this portion of the nozzle due to the adiabatic assumption.

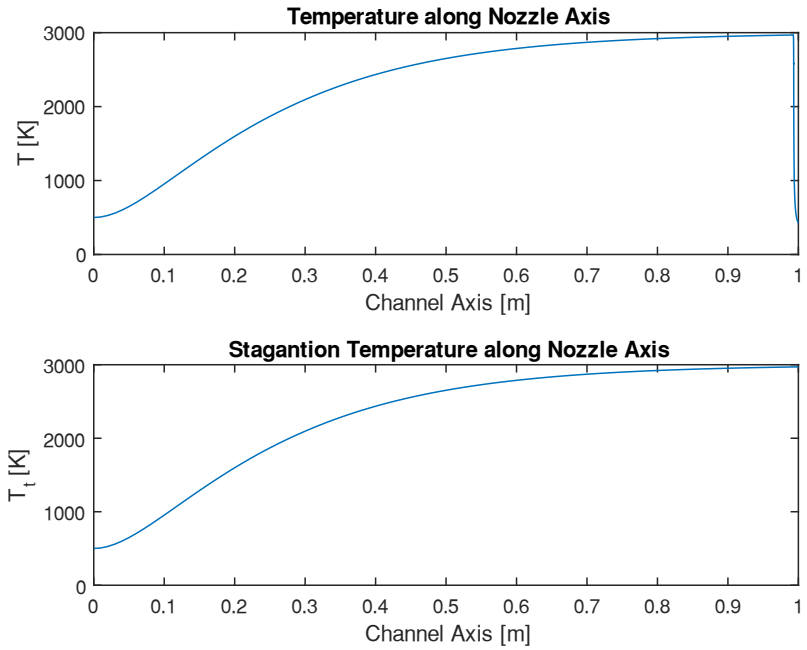

Figure 10: Static (upper) and Stagnation (lower) Temperature Profile along Channel Axis

The model also estimates the temperature at the inner radius of the coolant channel, which follows a profile similar to the one imposed at the outer radius, as merges from the comparison shown in Figure 11.

DOI: 10.13009/EUCASS2023-042

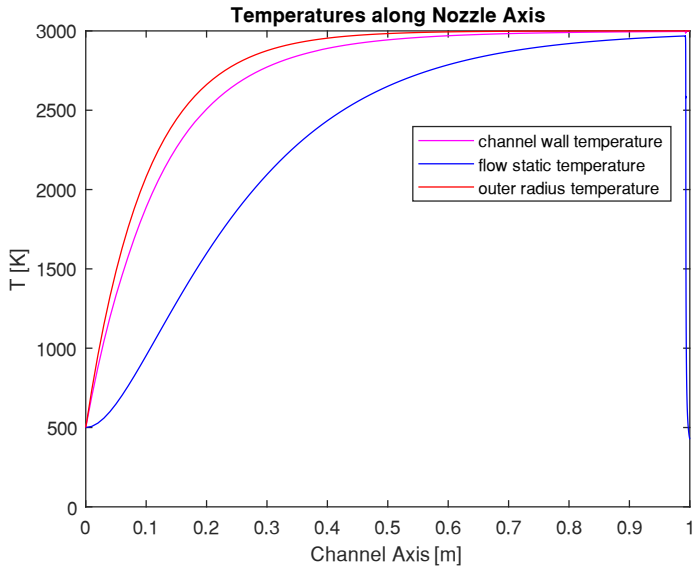

Figure 11: Flow and Duct Wall Temperature Profile

The power density profile represents another significant output of the model. The obtained shape of this profile would impose some requirements on the configuration of the fission nuclear reactor, and it is a pivotal factor of the iterative process on which to base the future multyphiscal analysis. Figure 12 shows the power density profile along the axis of the fuel element obtained after the imposition of the outer radius temperature profile, reported in Figure 5, as a boundary condition of the problem. The power density obtained does not have a sinusoidal shape like the one generally obtained in reactors with a configuration similar to that of the Rover/NERVA program. In the current case, the profile presents a steep increase at the channel's inlet and reaches its maximum value at 12% of the channel's total length. This profile follows a slow decrease until it reaches the nozzle's throat, where the smallest area enhances the heating exchange with the propellant requiring a small peak in the power density distribution. After the throat section, the adiabatic hypothesis on the supersonic part of the nozzle forces the power density to zero. A comparison of the estimated power density distribution with the ones published in the literature for different types of reactors [8,13] highlights how the obtained profile's shape is close to the one typical of the particle bed reactors [13–15]. This type of reactor has fuel elements composed of pellets storing the nuclear material on which the propellant flows. This configuration enhances the heat exchange between the fuel elements and propellant, allowing for reducing the total length of the core respect to a prismatic reactor configuration. This study points out a similar result. Figure 14 highlights the differences between the propellant flow stagnation temperature in the analyzed case (upper graph) and in the case with an applied sinusoidal power density profile to a prismatic core with nozzles integrated inside the coolant channels (lower graph). In the present scenario, the propellant reaches a temperature of about 2650 K at 50% of the fuel element length and 2890 K at 70% of that length, instead in the prismatic scenario, the flow reaches, at the same sections, a temperature of about 1700 K and 2400 K, respectively. Table *2* compares the performance obtained in the two cases, while Figure 14 overlaps their nozzle contours inside the coolant channels; almost negligible differences appear in the performance in terms of both thrust and specific impulse, and the channel contours are nearly the same. Therefore, the result of the above comparison highlights how the reactor configuration characterized by the power density profile obtained in this study can be the substitute for a prismatic reactor of the NERVA/Rover type to achieve fuel elements with a length reduced of about the 20%, and, consequently, the entire envelope of the propulsion system, while maintaining the same level of performance and the same nozzle geometry inside the channels. Table 2 also compares the performance obtained by the newly proposed configuration with multiple nozzles integrated inside the core’s coolant channels with the historic configuration having a single regeneratively cooled nozzle at reactor downstream collecting the flows coming from all the channels. This further comparison highlights how the multiple nozzles configuration gives the same propulsive performance as the classical one with a single regeneratively cooled nozzle but with a reduced length, limited to the core length.

DOI: 10.13009/EUCASS2023-042

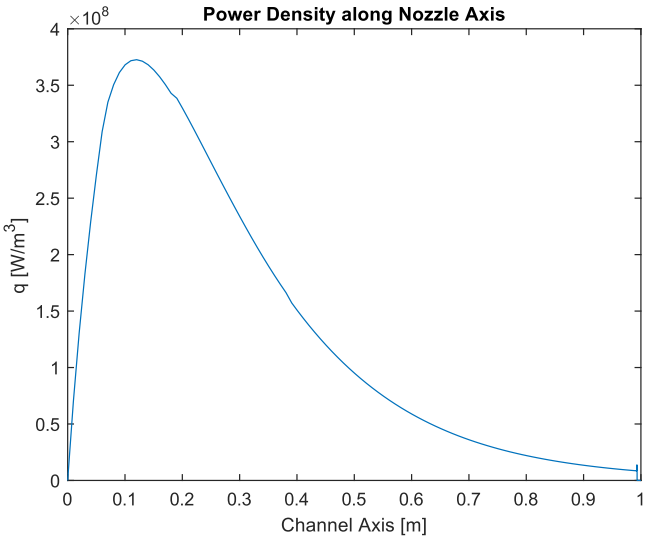

Figure 12: Core Power Density Profile Obtained from the Thermal-Hydraulics Analysis

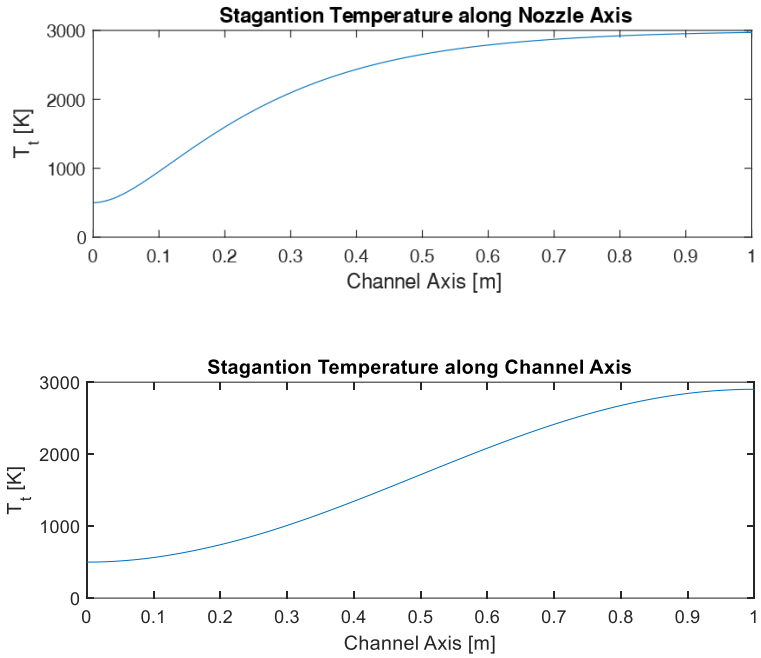

Figure 13: Analysed Case (upper) and Prismatic Fuel Element (lower) Stagnation Temperature Profiles along Channel Axis

DOI: 10.13009/EUCASS2023-042

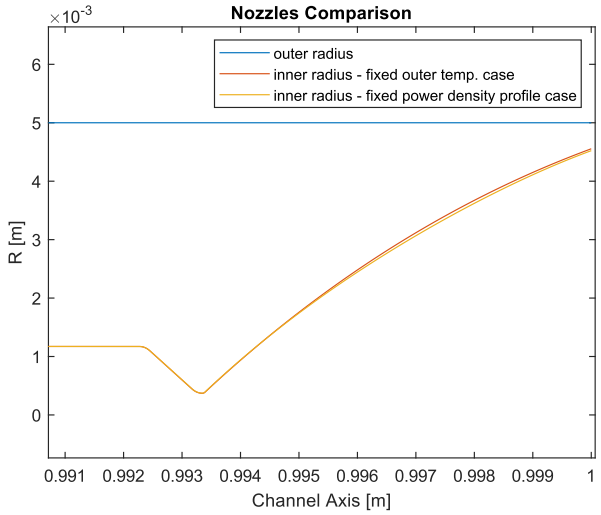

Figure 14: Fixed Power Density Profile and Fixed Outer Temperature Profile Geometry Comparison

Table 2: Multiple Nozzles Configurations and single Nozzle Historic Configuration Performance Comparison

	Multiple Nozzles (fixed T_{ro})	**Multiple Nozzles (fixed $P(z)$)**	**Single Nozzle**
Specific Impulse	324 s	320 s	320 s
Thrust/n° coolant channels	4.55 N	4.50 N	4.50 N
Length	1 m reactor	1 m reactor	1 m reactor 1 m thrust chamber 2 m nozzle

4. Conclusions

The proposed methodology focuses on the thermal-hydraulics part of the multiphysical analysis concerning a nuclear thermal rocket. This analysis does not fix the reactor geometry, as generally found in the literature, but determines the core configuration's main aspects starting from the propulsive performance. The innovative feature lies in the imposition of the Mach number profile and the channel outer temperature profile along the axis as a boundary condition of the problem of the propellant flowing through the core's coolant channel; the imposition of these two profiles reduces the systems of equations characterizing the problem in a square system easy to solve numerically. The results show how the adoption of an outer wall temperature profile having a fast asymptotic growth to the fuel-limiting temperature makes the propellant absorb more heat from the nuclear fuel in a shorter space, allowing a reduction of the core length compared to that of a core with a sine-shaped power density. The model furnishes the power density corresponding to the fixed temperature profile as an output, which appears to have a shape very close to the one characterizing the particle bed reactors. This result pushes for the adoption of this core configuration in the next steps of the analysis. The other main output of the model is the coolant channel contour with an integrated bell-shaped nozzle corresponding to the imposed Mach number profile. The obtained duct geometry allows the acceleration of the propellant flow up to such a point as to reach the same propulsive performance that would give a configuration with a single large nozzle downstream of the nuclear reactor, as done in most of the solutions proposed in the literature. However, this newly designed configuration reaches the same level of performance as the historic one with a significant reduction of the system envelope thanks to the elimination of the large nozzle. In conclusion, the results of the proposed new approach to face the thermal-hydraulic analysis of a nuclear rocket engine furnish the main elements for designing the propulsion system with a significatively reduced envelope compared to the historically proposed configurations.

DOI: 10.13009/EUCASS2023-042

References

[1] Porta, E. W., 1995, *Nerva-Derived Reactor Coolant Channel Model for Mars Mission Applications*, University of Nevada, Las Vegas.

[2] HOLMAN, R., and PIERCE, B., 1986, "Development of NERVA Reactor for Space Nuclear Propulsion," *22nd Joint Propulsion Conference*, p. 1582.

[3] Raepsaet, X., Proust, E., Gervaise, F., Baraer, L., Naury, S., Linet, F. L., Bresson, C. F., de Coriolis, C. C., Bergeron, I. T. A., and Bourquin, L. V., 1995, "Preliminary Investigations on a NTP Cargo Shuttle for Earth to Moon Orbit Payload Transfer Based on a Particle Bed Reactor," *AIP Conference Proceedings*, American Institute of Physics, pp. 401–408.

[4] Nam, S. H., Venneri, P., Kim, Y., Lee, J. I., Chang, S. H., and Jeong, Y. H., 2015, "Innovative Concept for an Ultra-Small Nuclear Thermal Rocket Utilizing a New Moderated Reactor," Nuclear Engineering and Technology, **47**(6), pp. 678–699.

[5] Powell, J., Maise, G., and Paniagua, J., 2002, "The Compact MITEE-B Bomodal Nuclear Engine for Unique New Planetary Science Missions," *38th AIAA/ASME/SAE/ASEE Joint Propulsion Conference & Exhibit*, p. 3652.

[6] DUKE, E., and VANICA, D., "Multiple Exhaust Nozzles for Nuclear Rocket Engines," *3rd Annual Meeting*, p. 925.

[7] Rao, G. V. R., 1958, "Exhaust Nozzle Contour for Optimum Thrust," Journal of Jet Propulsion, **28**(6), pp. 377–382.

[8] Emrich Jr, W. J., 2016, *Principles of Nuclear Rocket Propulsion*, Butterworth-Heinemann.

[9] Puccinelli, E., Aquaro, D., Pesetti, A., and Pasini, A., 2022, "Nuclear Thermal Propulsion for Earth Orbit and Interplanetary Missions: Challenges and Issues.," *73 Rd International Astronautical Congress (IAC)*, Paris, France, p. 17.

[10] Linstorm, P., 1998, "NIST Chemistry Webbook, NIST Standard Reference Database Number 69," J. Phys. Chem. Ref. Data, Monograph, **9**, pp. 1–1951.

[11] Hodge, B. K., 1999, "Using MathCad for Generalized One-Dimensional Compressible Flow in an Introductory Compressible Flow Course," *ASEE Annual Conference and Exposition, Session*, Citeseer.

[12] El-Wakil, M. M., 1971, *Nuclear Heat Transport.*, 1970.

[13] Li, X., Min, Q., Wu, X., and Liu, S., 2014, "Numerical Investigation of the Flow and Temperature Uniformity in the Reactor Core of a Pebble Bed HTGR Using Porous Media Method," *International Heat Transfer Conference Digital Library*, Begel House Inc.

[14] Balestra, P., Schunert, S., Carlsen, R. W., Novak, A. J., DeHart, M. D., and Martineau, R. C., 2021, "Pbmr-400 Benchmark Solution of Exercise 1 and 2 Using the Moose Based Applications: Mammoth, Pronghorn," *EPJ Web of Conferences*, EDP Sciences, p. 06020.

[15] Tyobeka, B., and Reitsma, F., 2010, "Results of the IAEA CRP5–Benchmark Analysis Related to the PBMR-400, PBMM, GT-MHR, HTR-10 and the ASTRA Critical Facility," *Proceedings of PHYSOR*, pp. 9–14.